Proceedings of ASME Turbo Expo 2022
Turbomachinery Technical Conference and Exposition
GT2022
June 13-17, 2022, Rotterdam, The Netherlands

GT2022-81929

AERODYNAMIC DAMPING PREDICTIONS DURING COMPRESSOR SURGE: A NUMERICAL COMPARISON BETWEEN A HALF AND FULL TRANSIENT APPROACH

Christoph Reiber, Virginie Anne Chenaux, Joachim Belz
German Aerospace Center
Institute of Aeroelasticity
Göttingen, Germany

ABSTRACT

The prediction of the aerodynamic damping during compressor surge is a challenging task, because the flow is continuously evolving along the four surge cycle phases: Pressurization (PR), Flow-Breakdown (FB), Reversed Flow (RF) and Regeneration (RG) and complex flow conditions like shocks and separations occur.

Damping predictions with current existing methods typically consist of two steps. In the first step a modified numerical model is used to simulate transient surge cycles. In the second step, damping analyses are performed for multiple timesteps along the surge cycle phases, which are then assumed as quasi-steady. The damping simulation can be performed using nonlinear or linear approaches. If shocks or separations occur, the latter yields inaccuracies in the flow and thus in the damping predictions.

A new approach was developed to take into account and improve these inaccuracies. This new method includes the damping prediction within the transient surge simulation. Thus, all surge cycle phases and the continuously evolving flow conditions are considered and nonlinear simulations are performed to account for shocks and separations. The results of this new method are presented and compared to the former method.

Keywords: axial-flow Compressor, surge modeling, numerical aeroelastic predictions, aerodynamic damping

NOMENCLATURE

FB	Flow-Breakdown
FTM	Full Transient Method
HTM	Half Transient Method
IBPA	Interblade Phase Angle
IGV	Inlet Guide Vane
PR	Pressurization
RF	Reversed Flow
RG	Regeneration
A_0	Blade Surface
E_{kin}	Kinetic Energy of Blade Vibration
$\vec{n}$	Surface Normal Vector
p	Static Pressure
T	Period Time of Blade Vibration
W_{ae}	Aerodynamic Work per Cycle
$\dot{\vec{x}}$	Time Derivative of Eigenvector
Λ_{ae}	Aerodynamic Damping log. Dec.

1. INTRODUCTION

The operating range of a compressor is typically presented in a performance map. The performance map shows the pressure ratio against massflow characteristic of the compressor for different speedlines. The operating range is for high pressure and low massflows limited by the surge line. If the operating conditions exceed the surge line different types of flow instabilities, like rotating stall or surge, occur. This behavior is described in detail by Willems and de Jager (1999), Paduano et al. (2001) and Day (2014). The type of the instability depends on the whole system configuration, Greitzer (1978). The instabilities lead to a drop-in compressor efficiency and may also to increased blade deformation and damage.

This study focuses on surge. In general, surge is a rapid transient flow instability, yielding an oscillation of the overall annulus averaged massflow in axial direction. Typically, surge is divided in four phases: Pressurization (PR), Flow-Breakdown (FB), Reversed Flow (RF) and Regeneration (RG). The transition between the phases is smooth. Starting from a low pressure high massflow operating condition within the pressurization phase, the flow is attached to the blade and air is accumulating in the system leading to an increase in pressure ratio and driving the operating conditions towards the surge line. If the operating conditions exceed the surge line the flow becomes unstable and the Flow-Breakdown phase starts. Within this phase the separation regions grow, the flow starts to reverse and the

pressure starts to discharge also in negative axial direction. In the third phase, the reverse flow is fully established, the massflow is dropped to a minimum and the pressure discharge rate is high. When the pressure in the system is low enough the flow starts to reattach to the blade and the regeneration starts. If the flow is fully reattached the surge cycle starts again with the pressurization phase. Figure 1 shows the characteristic of a mild surge and a deep surge in the compressor map. The strength of the reverse flow is dependent of the pressure rise of the compressor and the volume of the whole compression system.

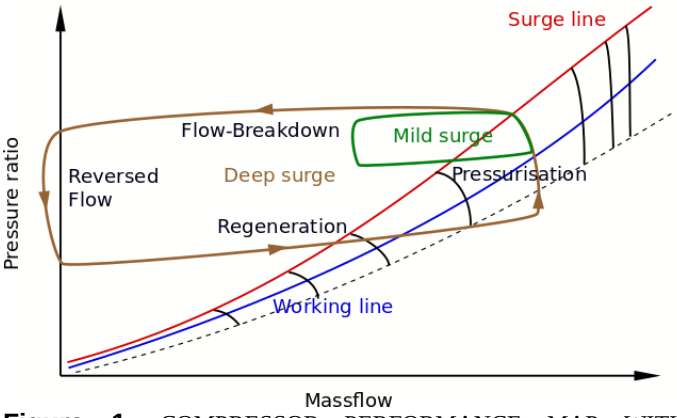

Figure 1: COMPRESSOR PERFORMANCE MAP WITH VARIOUS SPEEDLINES, MILD AND DEEP SURGE CYLES AND PHASES

Surge may lead to high blade deformations, damage and failure. Former studies have shown that flutter ([5], [6]) or forced response ([7]) could lead to high vibration amplitudes. This study is focused on flutter. The prediction of aerodynamic damping is a challenging task because the flow is strongly different in all surge cycle phases, the flow is rapidly changing between the phases and complex flow phenomena like separation and shocks occur. Two methods are already known to predict the aerodynamic damping during surge, one from Schönenborn [5] and one from L. Di Mare [6].

Schönenborn's method consists of two steps. In the first step a nonlinear steady-state simulation with inverted in- and outlet boundary conditions is used. The resulting flow field is assumed to represent the flow conditions during the RF phase. In the second step linearized damping simulations are performed for this flow field.

Di Mare's method consists of two steps as well. In the first step an extended numerical model is used for a transient simulation of multiple surge cycles. This model extension was firstly described by Vahdati [8]. In the second step multiple flow fields at different time steps along all surge cycle phases are extracted and nonlinear damping simulations are performed. The method used in this study, later called Half Transient Method (HTM) is based on the method from di Mare, but the damping simulation is linearized to ensure that the flow field remains unchanged. The HTM allows therefore the prediction of the damping at all phases of the surge cycle.

The advantage of both methods is that they give a fast prediction of the aerodynamic damping at specific timesteps during surge and thus are useful for design purposes. Nevertheless, both methods assume similar simplifications which might yield inaccuracies in the damping predictions. Both use linearized damping simulations and the flow field is considered quasi-steady. The continuously evolving flow conditions during surge are neglected. Furthermore, linearized damping analyses are used even if flow separation and shocks occur, which might lead to unphysical peaks in the damping prediction. To consider these features, a new method was developed overcoming both problems.

The new method, later called Full Transient Method (FTM), consists of only one step and uses the same model extension as the HTM to enable transient surge simulations. In contrast to the HTM, the blade deformation is included in the transient surge simulation. As a consequence, surge and blade deformation are present simultaneously, considering all surge cycle phases. The continuously evolving flow conditions are included and nonlinear simulations account for shocks and flow separations in order to improve the damping predictions.

The damping in the PR phase is expected to be positive because the flow conditions are more similar to stable operating conditions. Due to the complex flow fields at FB, RF and RG phase, strongly negative dampings might appear during specific surge cycle phases, leading to a timely localized blade flutter. As a consequence, for all IBPAs, the damping evolution along the different surge cycle phases have to be identified and monitored. If the surge averaged damping including all surge cycle phases is negative, flutter might occur over multiple surge cycles.

This study aims at presenting the first results of the novel FTM and comparing them with the HTM. The FTM results might show if negative aerodynamic damping is likely to occur, if flutter is possible over multiple surge cycles or only within critical surge cycle phases.

The comparison between both methods aims to show if the predicted damping evolution over time during one surge cycle and the surge averaged damping are at the same level. Moreover, the comparison helps determining if discrepancies can be identified and if the HTM can be applied to design purposes. Discrepancies are expected especially during the FB, RF and RG phase, where flow separations and reversed flows occur. A good agreement is expected for the PR phase where the flow fields are more similar to the stable operating conditions. The comparison might also highlight in which of the surge cycle phases the HTM can be used with high confidence.

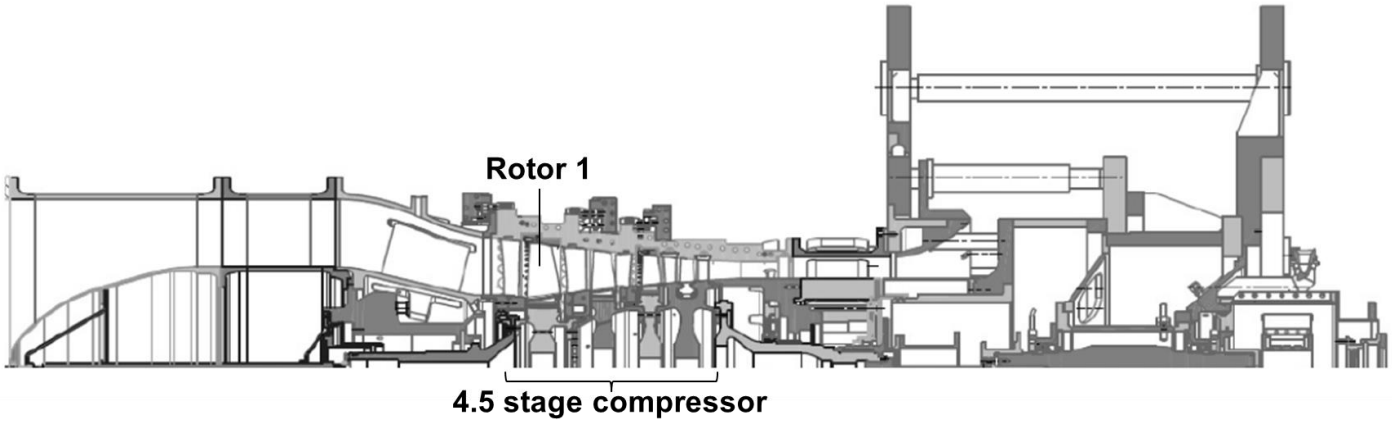

Figure 2: DLR Rig250 research compressor, 4.5 stage configuration

2. MATERIALS AND METHODS

2.1. Numerical Model

The compressor domain was extracted from the transonic DLR research compressor RIG250 (Figure 2). The normal 4.5 stage configuration with inlet guide vanes and two variable stator vanes was reduced to the first stage only (with IGV) to ensure reasonable CPU times.

Figure 3 presents the numerical setup. In the downstream direction the compressor domain is extended by an outlet pipe and a laval nozzle. In the upstream direction an inlet domain was added together with a bypass outlet.

The throttle part of the laval nozzle is choked and defines the massflow through the system. The throttle area is kept constant within one simulation. Over multiple simulations the throttle area is decreased, leading to a change in compressor operating conditions towards surge. For a so-called critical throttle area, the surge line is crossed, the flow becomes unstable and the whole system surges. The outlet pipe defines the surge volume and can be used in combination with the throttle area to adapt the systems surge behavior. The diffusor part of the throttle area is shocked to provide subsonic outflow conditions for the flow solver. The inlet domain includes the global inlet and an extra bypass outlet. The bypass outlet allows the flow at reverse flow conditions to leave the system and keep a forward flow at the global inlet. A detailed description of the systems behavior can be found in Reiber [9].

For steady-state and unsteady simulations all rows are modeled as a single passage. Each passage has approximately one million cells, leading to an overall cell count of 4.1 million cells for the whole model. The grid resolution was selected to the best engineering knowledge and judgement. The interfaces between IGV-rotor and rotor-stator are considered as mixing planes, so that the flow is kept circumferentially symmetric. This setup does not enable the occurrence of local rotating stall cells and might thus lead to inaccuracies in the accurate prediction of the surge onset. Nevertheless, since surge is an instability affecting the total system volume, it can be considered of axisymmetric nature. The method is therefore particularly appropriate to predict the main features of the surge cycles. The other interfaces are modeled as zonal interfaces, so that the flow parameters are transferred directly. All simulations are done for 100% rotational speed (12960 rpm). The total pressure, total temperature, flow angles and turbulence parameter are imposed at the Atmospheric inlet and the static pressure is prescribed at both outlets.

2.2. Half Transient and Full Transient Damping Analysis

In this study, the aerodynamic damping is defined as the logarithmic decrement computed from the aerodynamic work per cycle W_{ae} and the kinetic energy E_{kin} of the blade vibration:

$$\Lambda_{ae} = \frac{W_{ae}}{2E_{kin}} \tag{1}$$

Thereby the aerodynamic work per cycle W_{ae} is defined as the integral over the blade surface A_0 and one blade vibration period T of the product of static pressure p, the normal vector $\vec{n}$ and the time derivative of the eigenvector $\vec{x}$:

$$W_{ae} = \int_0^T \int_0^{A_0} p \cdot \vec{n} \cdot \dot{\vec{x}} \, dA \, dt \tag{2}$$

To get the surge averaged damping the arithmetic average of the aerodynamic damping per cycle is evaluated over one surge period.

The first step for both HTM and FTM damping methods is a transient surge simulation to identify the system surge behavior. The massflow evolution over time shows the surge frequency,

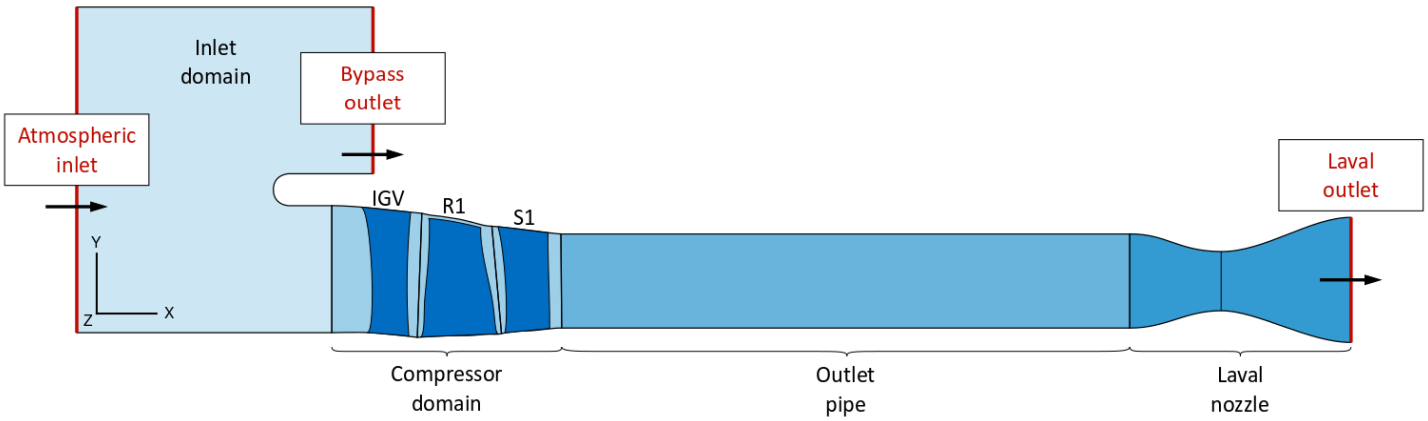

Figure 3: NUMERICAL SETUP OF RIG250, IGV + STAGE 1 CONFIGURATION WITH INLET DOMAIN, COMPRESSOR, OUTLET PIPE AND LAVAL NOZZLE

the minimal massflow at reversed flow conditions and its progression along the different surge cycle phases.

For the HTM, multiple flow fields at different timesteps along the surge cycle phases are then extracted from the transient surge simulation. In a second step, linearized damping simulations are performed for every timestep of interest. The base flow is kept unchanged and the linearization provides the harmonic pressure fluctuations due to the blade vibration. For the aerodynamic damping analysis, a numerical model with a single passage consisting of the rotor only is used. The result of each linearized simulation is a single damping value for a specific mode, IBPA and timestep. The aerodynamic damping is predicted only for a reduced number of timesteps and the results from the single time steps have to be combined to get the damping evolution over time along the different surge cycle phases.

For the FTM, the setup is extended by a forced blade motion with constant oscillation amplitude. All rotor passages have to be included in the numerical setup in order to apply the rotors deformation to different IBPAs as well as the surge conditions simultaneously. The model consists of 30 million cells for this configuration. For each mode and each IBPA one unsteady simulation has to be performed. The result of each simulation is the continuously aerodynamic damping evolution over time for a specific mode and IBPA. The damping value is determined using the time data gathered from the last blade vibration cycle. with Equation 1. Thereby, only the pressure fluctuation due to the blade vibration is considered.

All simulations were performed with the DLR Turbomachinery flow solver TRACE [10]. The TRACE nonlinear module and LinearTRACE were applied for the steady-state and nonlinear damping simulations, and for the linearized damping simulations respectively. The Wilcox-k-w turbulence model and frozen turbulence parameters were imposed for the nonlinear and linearized simulations respectively.

3. RESULTS AND DISCUSSION

This section starts with the presentation of the transient surge behavior which is the basis for both damping predictions. The second part presents the comparison of the predicted surge averaged damping and for two IBPAs the damping evolution over time between both methods. Finally, the results of the FTM are detailed.

3.1. Transient Surge Simulation

The first step to undertake a surge simulation is to determine the critical throttle area. For the numerical model used in this study, throttle areas of 64% and higher ensure stable operating conditions whereas for throttle areas lower than 64%, surge occurs. Therefore, in this study, all simulations were performed with a throttle area of 63%.

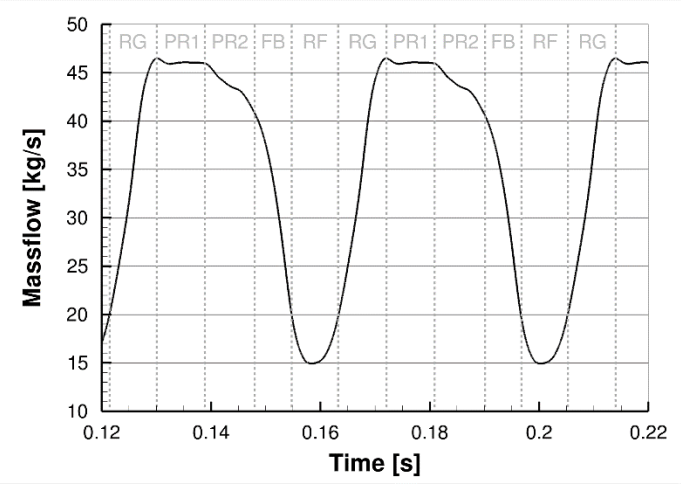

Figure 4: MASSFLOW AT ROTOR INLET OVER TIME FOR MULTIPLE SURGE CYCLES WITH SURGE CYCLE PHASES

For this throttle area, an unsteady nonlinear simulation without blade deformation was performed. A total of five identical surge cycles were simulated. Figure 4 shows the time evolution of the massflow at the rotor inlet for the last two complete surge cycles.

The four different surge cycle phases Pressurization (P), Flow-Breakdown (FB), Reversed Flow (RF) and Regeneration (RG) are identified in the figure. The pressurization phase is divided in two parts PR1 and PR2, because the massflow evolution differs strongly between both parts. Whereas in PR1 the massflow is nearly constant, in PR2 it is decreasing until the flow breaks down.

The surge frequency is 23,9 Hz and the minimum massflow in the reversed flow phase is 32,6% of the design massflow. Since the numerical model is reduced to IGV and first stage, the pressure ratio is limited and no deep surge with a fully spanwise reversed flow occurs. Nevertheless, a local reversed flow occurs which spreads from the rotor tip to the hub (Figure 5).

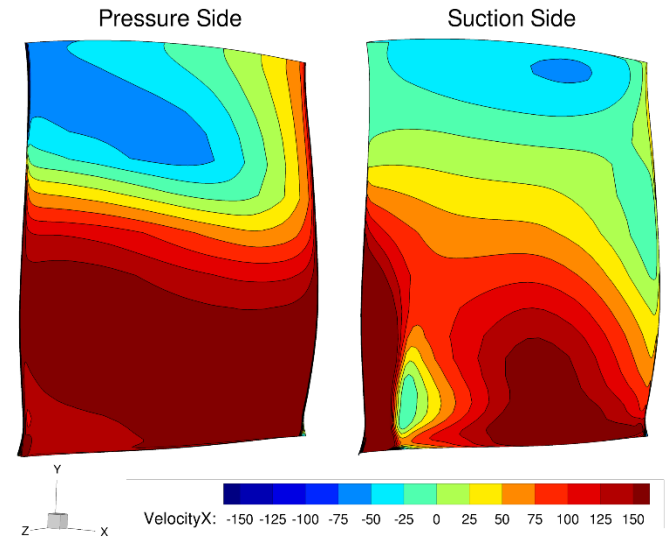

Figure 5: BLADE SURFACE AXIAL VELOCITY AT BLADE PRESSURE AND SUCTION SIDE DURING REVERSED FLOW

3.2. FTM vs. HTM: Surge Damping Diagram

For this study damping predictions were performed for the blade's first modeshape (first bending) and all 24 IBPAs. The FTM simulates 65536 timesteps over 5 surge cycles. 24 transient surge simulations with simultaneous blade deformation were carried out (one for each IBPA). For the HTM, 256 timesteps over the last three surge cycles were considered. A total of 6144 linearized damping simulation were performed. The HTM uses 650 CPU hours for each mode and IBPA and the FTM uses 7500 CPU hours. This corresponds to a factor 10 and shows in which extent the FTM is more expensive in terms of CPU time and how much CPU hours can be saved if the HTM can be applied for specific cases where its accuracy is guaranteed.

Figure 6 presents the surge averaged damping diagram for the FTM (solid line) and HTM (dashed line). There is a fair agreement between both methods over the IBPAs, meaning that the flutter stability over multiple surge cycles is predicted at a similar level for both methods. Furthermore, the damping stays positive for all IBPAs and no flutter over multiple surge cycles occurs. At a first glance, it seems that the accuracy of the HTM is very good and that the HTM is a promising tool for design purposes. The next step takes a closer look on the damping evolution along the different surge cycle phases. Two IBPAs were compared: the first is IBPA -15° because it has a low damping for both methods and large discrepancies appear between both methods. The second is IBPA -75° because the averaged surge averaged dampings are similar for both methods.

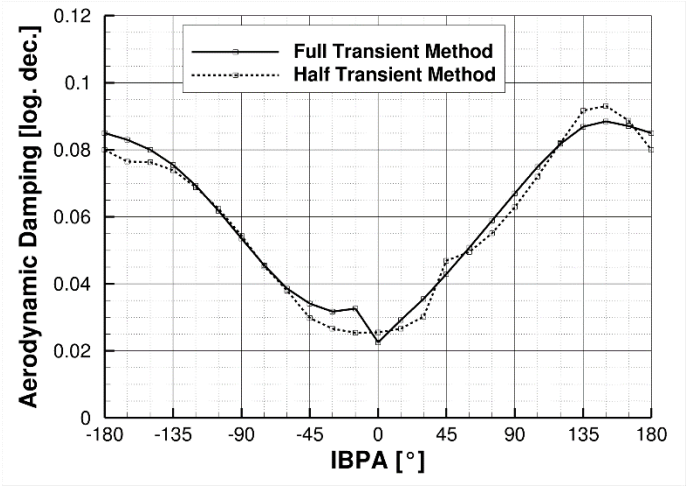

Figure 6: SURGE AVERGAGED DAMPING WITH FULL AND HALF TRANSIENT METHOD FOR THE FIRST BLADE MODE (FIRST BENDING)

3.3. FTM vs. HTM: Damping evolution along surge cycle phases

Figure 7 shows the damping evolution along the different surge cycle phases for the HTM and FTM. IBPA -15° and IBPA -75° are depicted on the left and right side respectively. The black lines show the aerodynamic damping and the red lines show the surge averaged damping. The solid lines present the FTM and the dashed lines present the HTM. The surge averaged damping values from Figure 6 are visible in the red lines.

For IBPA -15° (Figure 7A), the damping evolution over time shows a fair agreement at the end of the PR2 phase, for the FB and RF phase and at the beginning of the RG phase, but strong discrepancies at the end of the RG phase as well as in the PR1 phase. The FB, RF and RG phases are characterized by separation regions and complex flow conditions. During these phases a stronger discrepancy between both methods was expected. In contrast during the phases PR1 and PR2 the flow is more similar to the flow conditions for stable operating point and a better agreement was expected.

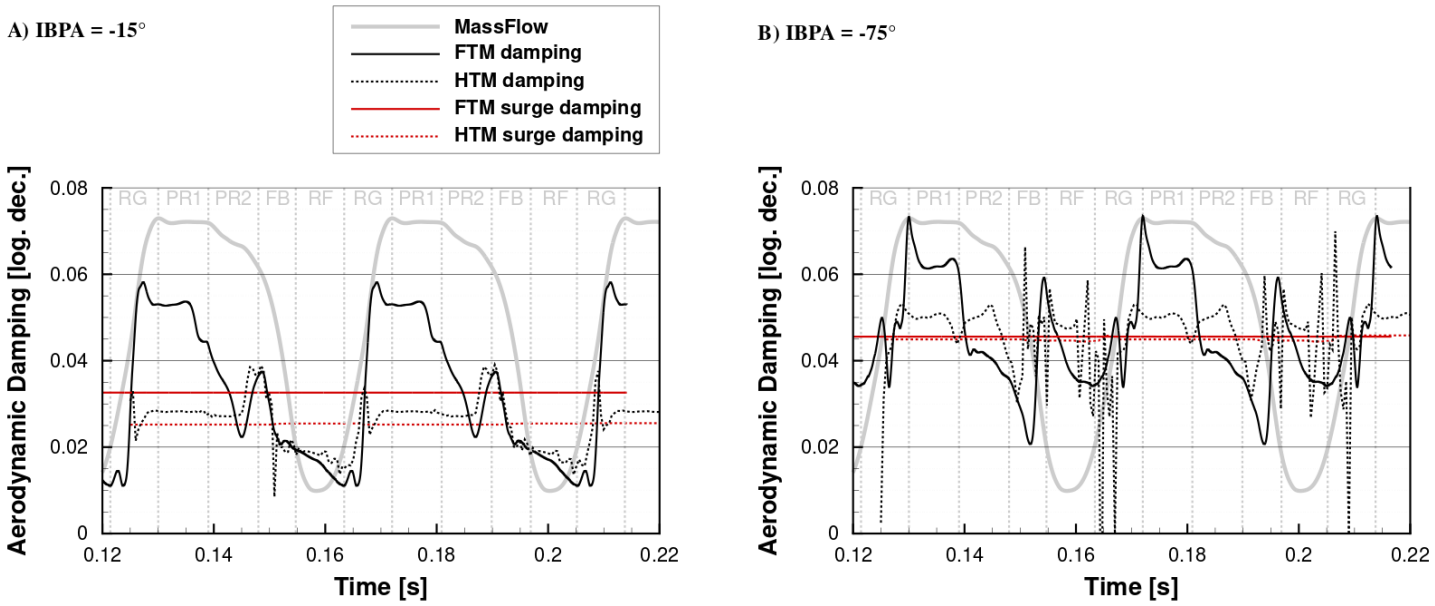

Figure 7: AERODYNAMIC DAMPING EVOLUTION OVER TIME FOR HTM AND FTM, A) IBPA -15°, B) IBPA -75°

A detailed analysis of the unsteady aerodynamic prediction during the PR1 phase should be carried out in order to provide a better understanding of the sources associated to these discrepancies.

Furthermore, there is a strong peak with very low damping in the FB phase for the HTM. This peak is not present during the second surge cycle. This might enhance an inaccuracy due to the linearized approach of the damping simulation.

For IBPA -75° (Figure 7 B), the damping evolution over time strongly differs between HTM and FTM along all surge cycle phases. The discrepancies compensate each other over time, leading to the good agreement in the surge averaged damping values.

The HTM shows peaks and negative damping, especially in the FB, RF and RG phases where flow separations are present. These peaks are most likely due to the linearized damping analysis and might be purely numerical. The FTM shows a much smoother curve in these phases. Furthermore, the peaks do not appear at the same times for the second surge cycle, because they were evaluated at various timepoints with respect to the surge cycle. This highlights that the result is very sensitive to small time differences in the sampling.

For this IBPA, it can be observed that a good agreement in the surge averaged damping does not guarantee a good agreement in the damping evolution along the different surge cycle phases. A more detailed analysis of the 3D unsteady aerodynamics is necessary to evaluate where the HTM can be applied with high confidence intervals.

3.4. Full Transient Method: damping evolution for different IBPAs

Figure 8 presents the evolution of the aerodynamic damping along the surge cycle phases for multiple IBPAs. Although all IBPAs are simulated, only every second IBPA is presented to ease the visualization. Figure 8 A) includes the IBPAs from -135° to -45° B) from -45° to +45 C) from +15° to +135° and D) from +135° to +225°/-135°.

The figure shows that the aerodynamic damping stays positive for all IBPAs along the surge cycle phases. No flutter occurs for specific surge cycle phases, not even in the RF phase.

For all IBPAs the damping levels are dropping in the FB, RF and RG in contrast to the PR1 and PR2. The minima mostly occur during the RF phase and are very close to the unstable region (Figure 8B). Unlike the HTM, the transitions between the IBPAs are smooth and there are no peaks in the damping curves.

The figure shows also that there are basically two types of damping evolution over time. They repeat for different IBPAs at different damping levels (Figure 8A and C). These differences in the overall damping level are also leading to the differences in the surge averaged damping. Therefore, it can be noted that, the main differences in the surge averaged damping for the various IBPAs are mainly driven by an overall change in the damping level and not by specifically high or low damping levels during the surge cycle phases.

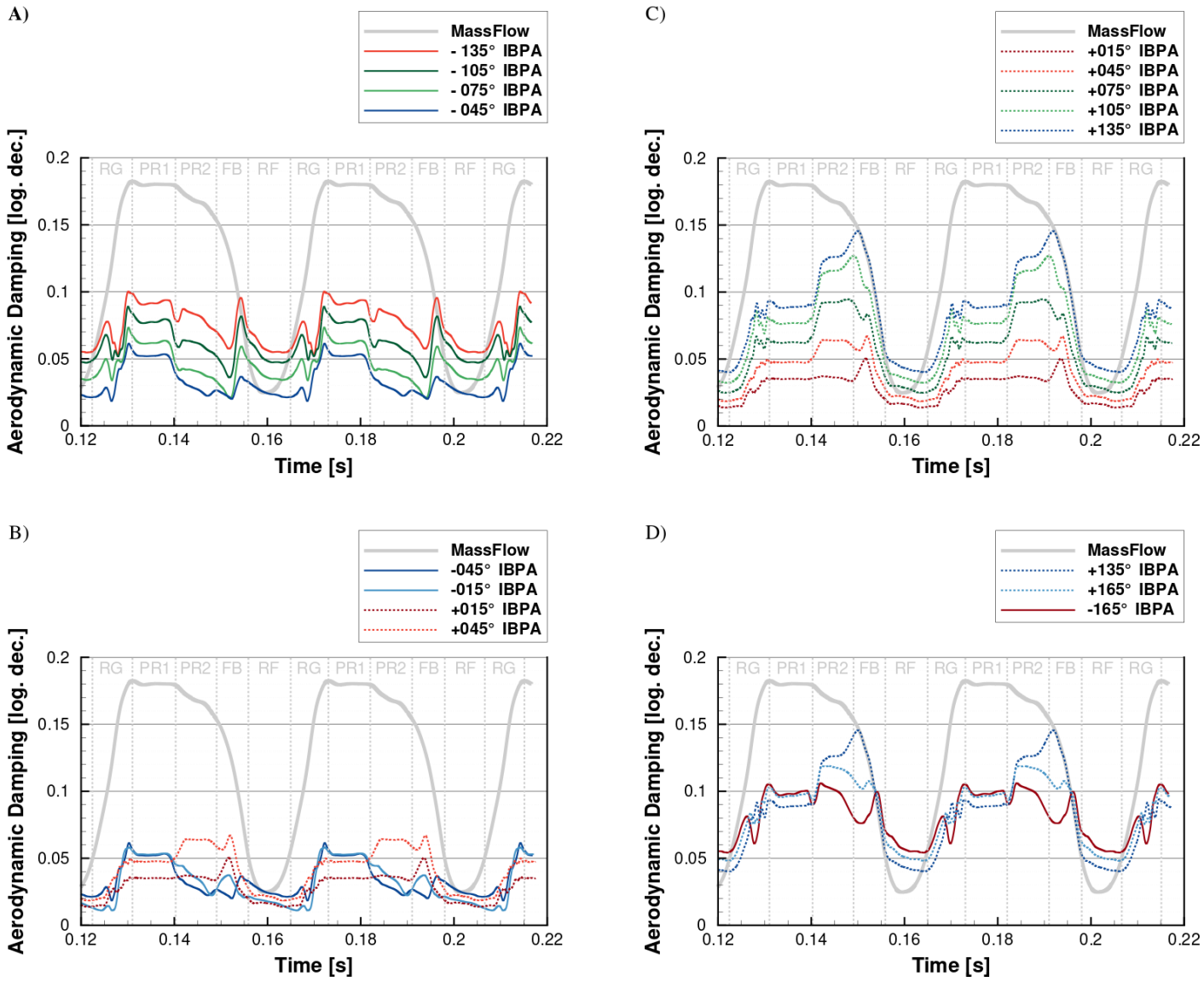

Figure 8: AERODYNAMIC DAMPING OVER TIME FOR FTM FOR DIFFERENT IBPAS, A) -135° to -45° B) -45° to +45° C) +15° to +135° D) +135° to +225° (-165°)

The damping evolution for the IBPAs with the lowest (Figure 8B) and highest surge averaged damping values (Figure 8D) show that these values are also driven by an overall increased or decreased damping level and not by specifically high or low peaks.

4. CONCLUSION

A novel Full Transient Method was developed for the aerodynamic damping predictions during compressor surge. The first results are presented and compared to a Half Transient Method.

Therefore, an extended numerical model with IGV and first stage of the DLR RIG250 compressor was used. The damping prediction was performed for the rotor first mode and all IBPAs. The surge averaged damping shows a good agreement between both methods, meaning that the HTM might be promising and sufficient for design purposes. For some IBPAs, the averaged damping is close to the unstable region but remains positive, meaning that no flutter is present over multiple surge cycles.

The damping evolution over time for an entire surge cycle and its different surge cycle phases was compared for two IBPAs. The comparison shows that a good agreement in the surge averaged damping does not guarantee a good agreement in the damping evolution over time. Strong discrepancies can be

observed in the damping evolution for all surge cycle phases and the methods not only differ for the critical surge cycle phases (FB, RF, RG), they also differ during the pressurization phase (PR1 and PR2), where a good agreement was expected. A detailed analysis of the 3D unsteady flow would be necessary to explain these discrepancies. Furthermore, the HTM shows strong peaks in the damping evolution over time which might be purely numerical and might lead to erroneous flutter predictions.

A detailed look at the FTM results show that the damping stays positive during all surge cycle phases. Furthermore, the damping evolution over time is smoothly changing between the IBPAs. The evolution is smooth along the surge cycle phases as well and shows no unphysical peaks. This highlights that the differences in the surge averaged damping are mainly due to a change of the overall damping level and not to specifically high or low damping levels during the surge cycle phases. The most critical surge cycle phase is the RF phase. The damping during the PR phase is higher and has a stabilizing effect on the surge averaged damping.

5. OUTLOOK

A similar study with a reversed flow along the full blade span should be performed to see if there are differences in the flow predictions and in the aerodynamic damping.

The new method should be validated against experimental results. Particularly, the correct prediction of surge onset, flow separation and flow reattachment, have an influence on the aerodynamic damping: this should be validated as well.

REFERENCES

[1] Paduano J.D., Greitzer E.M., Epstein A.H., 2001, "Compression System Stability and Active Control", Annual Rev. Fluid Mech. 2001, Vol. 33.

[2] Willems F., de Jager B., 1999, "Modeling and Control of Compressor Flow Instabilities", IEEE control systems, Vol. 19 (Issue 5).

[3] Day I. J., 2016, "Stall, Surge, and 75 Years of Research", Journal of Turbomachinery, Vol. 138.

[4] Greitzer E. M., 1978, "Surge and Rotating Stall in Axial Flow Compressors, Part I and Part II: Theoretical Compression System Mode ", ASME Journal of Engineering for Power, Vol.98.

[5] Schönenborn H., Chenaux V., Ott P., 2011, "Aeroelasticity at Reversed Flow Conditions – Part 1: Numerical and Experimental Investigations of a Compressor Cascade with Controlled Vibration", Proceedings of ASME Turbo Expo.

[6] di Mare L., Krishnababu S.K., Mück B., Imregun M., 2009, Aerodynamics and aeroelasticity of a HP compressor during surge and reversed flow", Proceedings of the ISUAAAT, vol. 12.

[7] Giersch T., Figaschewski F., Hönisch P., Kühhorn A., Schrape S., 2014, "Numerical Analysis and Validation of the Rotor Blade Vibration Response Induced by High-Pressure Compressor Deep Surge", Proceedings of the ASME Turbo Expo Conference, Düsseldorf, Germany (GT2014-26295).

[8] Vahdati M., Sayma A. I., Freeman C., Imregun M., 2005, "On the Use of Atmospheric Boundary Conditions for Axial-Flow Compressor Stall Simulations", Journal of Turbomachinery, Vol. 127, pp. 349-351.

[9] Reiber C., Chenaux V., 2019, "Numerical analysis of the influence of surge behavior on the flutter stability of compressor blades", Proceedings of the 13th ETC

[10] Kersken H.-P., Frey C., Voigt C., Ashcroft G., 2012, "Time-Linearized and Time-Accurate 3D RANS Methods for Aeroelastic Analysis in Turbomachinery". Journal of Turbomachinery, Vol. 134.